CrystEngComm

Accepted Manuscript

ROYAL SOCIETY OF CHEMISTRY

www.rsc.org/crystengcomm

Journal Name RSCPublishing

ARTICLE

Structural diversities and magnetic properties of azide-containing coordination polymers based on flexible tetra-pyridinate ligands

Cite this: DOI: 10.1039/x0xx00000x

Received 00th January 2012,
Accepted 00th January 2012

DOI: 10.1039/x0xx00000x

www.rsc.org/

Fan Yu,[a,*] Mi Xiang,[a] Ai-hua Li,[a] Yu-min Zhang,[a] Bao Li[b,*]

Abstract: By utilizing two similar flexible quadrictopic ligands, tetrakis(4-pyridyloxymethyl)methane (4-TPOM) and tetrakis(3-pyridyloxymethyl)methane (3-TPOM), four new azido-containing coordination polymers with the formula $[Mn_3(4\text{-}TPOM)_3(N_3)_6(H_2O)_6]_n$ (1), $[Ni(4\text{-}TPOM)(N_3)_2]_n$ (2), $[Mn(3\text{-}TPOM)_2(N_3)_2(H_2O)_3(CH_3OH)_4]_n$ (3) and $[Co(3\text{-}TPOM)(N_3)_2]_n$ (4) had been synthesized and structurally characterized. Compound **1** shows 1D helical chain comprised of six-coordinated Mn^{II} geometries and two-connected tetra-pyridinate ligands. Compound **2** exhibits a three-dimensional framework based on 1D Ni(II) chains with alternating double end-to-end (EE) and double end-on (EO) azide bridges and tetrapyridyl ligands in a highly-distorted conformation. Compound **3** shows 2D layer comprised of six-coordinated Mn^{II} geometries with mono-dentate azide ions and two types of two-connected tetra-pyridinate ligands. Compound **4** exhibits a three-dimensional framework based on 1D Co(II) chains with double end-to-end (EE) azide bridges and tetrapyridyl ligands in a cross-shaped conformation. Magnetic investigations on complexes **2** and **4** revealed antiferromagnetic interactions through the bridged azide ligands. In addition, the magnetic measurement manifest that **2** exhibits weak antiferromagnets, which might be caused by the spin canting.

Introduction

In recent years, azide-containing coordination polymers (CPs) have received considerable attention due to the interest in constructing new molecular magnets with interesting magnetic properties.[1–4] The azido ligand plays an important role in this filed due to not only in its diverse bridging modes but its strong efficient magnetic coupling. The azido ligand effectively mediates ferromagnetic interactions in an end-on (EO) mode, and antiferromagnetic interactions when it bridges in an end-to-end (EE) mode.[2] Versatile azido-bridged polymers with different dimensionality and topological structure had been synthesized by utilizing various auxiliary ligands, such as 4,4'-bipyridine, pyrazine and some other bi-pyridyl derivatives and a great diversity of magnetic behaviors have been demonstrated.[1-6] These bi-pyridyl derivatives tend to interlink the inorganic metal-azide chains or layers to generate multidimensional materials. Nowadays, it is believed that bulk-like magnetism could be triggered or enhanced by increasing the dimensionality of magnetic polymers.[7] Therefore, the rational construction of high-dimensionality, especially 3D, metal-azido CPs is attractive and still poses a great challenge. Compared to the high-dimensionality magnetic CPs constructed by azido bridging ligands with bi-pyridyl ligands, 3D metal-azide systems with tetra-pyridyl ligands had been rarely investigated.[8] Among these tetra-N-containing ligands, 4-TPOM (4-TPOM = tetrakis(4-pyridyloxymethylene)methane), an important flexible tetra-dentate ligand, whose four pyridyl arms could twist around the central quaternary carbon atom randomly, would be a good candidate for the construction of azide-containing CPs with diverse structures.[9-11] To further explore the potential of this type of flexible ligands, we changed the *p*-position of the N atoms of the pyridine rings to the *m*-position, and generated a new tetra-pyridine ligand, tetrakis(3-pyridyloxymethyl) methane (3-TPOM). Compared to the flexibility of 4-TPOM, 3-TPOM would adopt much more variable conformations because of the additional rotation of the pyridine rings, illustrated in Scheme S1, leading to much more unpredictable CPs.[11] Therefore, these neutral flexible ligands would easily result in variable CPs with azide-anion. With all the above considerations in mind, we reported the synthesis and characterization of four new azide-containing CPs assembled from these tetra-pyridines linkers, namely, $[Mn_3(4\text{-}TPOM)_3(N_3)_6(H_2O)_6]_n$ (1), $[Ni(4\text{-}TPOM)(N_3)_2]_n$ (2), $[Mn(3\text{-}TPOM)_2(N_3)_2(H_2O)_3(CH_3OH)_4]_n$ (3) and $[Co(3\text{-}TPOM)(N_3)_2(H_2O)_4]_n$ (4). These new compounds are characterized by elemental analysis, IR spectra, magnetism and X-ray crystallography. The crystal structures and magnetic analyses of these compounds are presented in detail.

Results and discussion

Synthesis of CPs 1–4

Journal Name RSCPublishing

ARTICLE

Table 1. crystal data of 1 - 4

	1	2	3	4
Chemical formula	$C_{75}H_{84}Mn_3N_{30}O_{18}$	$C_{25}H_{24}Ni_2N_{16}O_4$	$C_{51}H_{58}MnN_{14}O_{12}$	$C_{25}H_{24}Co_2N_{16}O_4$
Formula Mass	1858.50	729.95	1114.03	730.46
Crystal system	Trigonal	Monoclinic	Monoclinic	Tetragonal
a/Å	9.61970(10)	11.4110(2)	16.2734(18)	10.29180(10)
b/Å	9.61970(10)	11.9654(2)	18.977(3)	10.29180(10)
c/Å	28.4217(9)	20.9225(5)	19.136(2)	33.1588(8)
β/°	90.00	98.418(2)	111.964(14)	90.00
Unit cell volume/Å3	2277.74(8)	2825.92(10)	5480.7(12)	3512.22(10)
Temperature/K	293(2)	293(2)	293(2)	293(2)
Space group	$P3_121$	$C2/c$	$P2_1/c$	$I4_1/a$
Z	1	4	4	4
No. ref	19226	7532	25171	7907
Rint	0.0318	0.0195	0.0502	0.0298
Final R1 values (I > 2σ(I))	0.1043	0.0417	0.0469	0.0469
Final R1 values (all data)	0.1111	0.0447	0.1023	0.0607

The crystalline compounds were synthesized from the solvothermal reaction of different metal salts, NaN_3 and 4-TPOM or 3-TPOM in the mixed solvent of methanol and water, and their crystal data were listed in Table 1. In the IR spectrum, the characteristic absorption peaks of the azide group and other functional ones were clearly presented. The strong absorption bands around 2070 and 1350 cm^{-1} are assigned to the asymmetric or symmetric azide vibration. The strong bands in the regions of 1620–1450 cm^{-1} are assignable to the pyridine group.

Crystal structure of 1

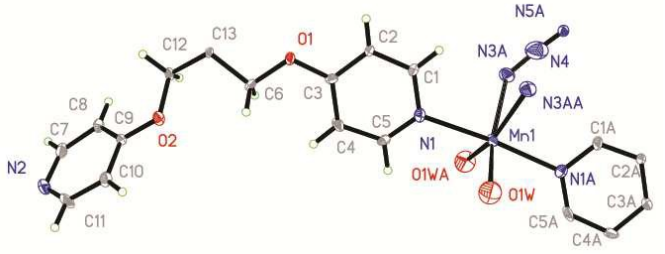

Figure 1. the perspective view of asymmetric unit of **1** with 30% probability level.

The X-ray single crystal diffraction study indicates that **1** crystallizes in the trigonal crystal system $P3_121$, and shows a one dimensional helical structure resulting from the connecting of manganese atoms through slightly-distorted tetrahedral 4-TPOM ligand. The asymmetric unit contains a Mn ion located on a crystallographic inversion center, one coordinated aqua molecule, one independent azide ion and half 4-TPOM ligand (Figure 1). The central manganese atom adopts the octahedral geometry and is coordinated by four N atoms and two coordinated aqua molecules. The axial positions are occupied by two pyridyl rings of different tetra-pyridinate ligands, while the adjacent equatorial positions are occupied by two coordinated water molecules and two coordinated azide ions, shown in Figure 2. The Mn-$N_{pyridine}$ or -N_{azide} and Mn-O_{aqua} bond lengths fall in regions of 2.270 to 2.396 Å, respectively, in accordance with the typical values of manganese(II) state.

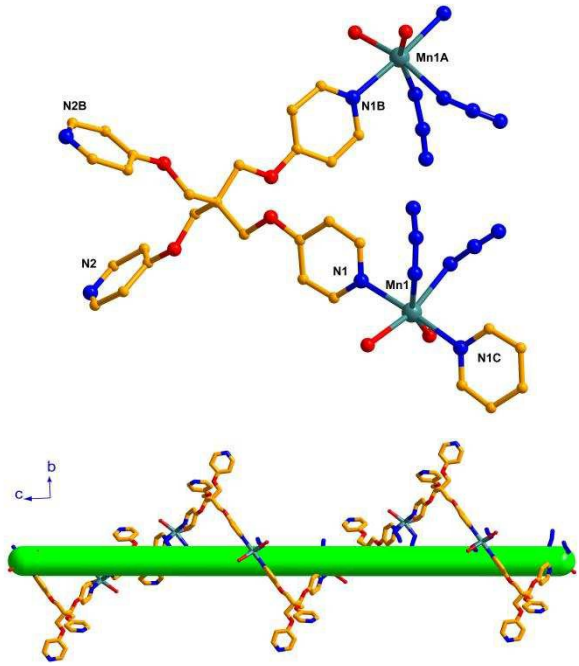

Figure 2. Up) the coordination modes of the tetra-pyridinate ligand and the central Mn ion; Down) 1D helical chain of 1 along c-axial direction(Green line represents the helical axis).

For **1**, the inherently flexible tetrapyridyl ligand 4-TPOM ligand adopts a slightly distorted tetrahedral conformation of the four pyridyl groups with N···$C_{central}$···N angles ranging from 156.40(20)° to 158.95(15)°. Each 4-TPOM ligand utilizes the adjacent two pyridyl arms to link two Mn(II) ions with Mn···Mn distance of 11.223 Å, and the opposite coordinate sites of each Mn atom are further occupied by pyridyl N atoms to form 1D helical chain, shown in Figure 2. The remained

pyridyl N atoms in one chain are left to contact with oxygen hydrogen atoms of other helical chains with the distance of 2.794 Å to form the 3D supramolecular structure.

Crystal structure of 2

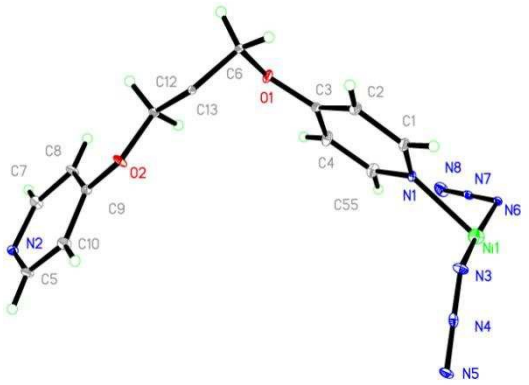

Figure 3. the perspective view of asymmetric unit of **2** with 30% probability level.

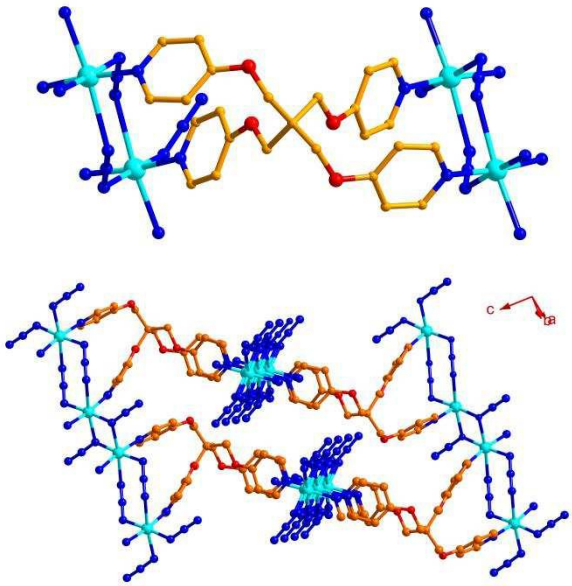

Figure 4. Up) the coordination modes of the tetra-pyridinate ligand and the central Ni ion; down) 3D structure of compound **2** based on 1D nickel-azide chains (hydrogen atoms are omitted for clarity), showing the different orientation.

X-ray single crystal diffraction studies reveal that **2** crystallizes in the monoclinic crystal system *C*2/c, and shows a three dimensional structure resulting from the connecting of 1D Ni□-azide neutral chains with alternating double EE and EO azide bridges through highly-distorted 4-TPOM ligand. The asymmetric unit contains an independent nickel ion, two independent azide ions and half 4-TPOM ligand (Figure 3). The central nickel atom adopts the octahedral geometry. The axial positions are occupied by two pyridyl rings of different tetra-pyridinate ligands, while the equatorial positions are occupied by four N atoms of two EE and two EO azide ions. The Ni-$N_{pyridine}$ and Ni-N_{azide} bond lengths fall in regions of 2.081 to 2.143 Å, respectively, in accordance with the typical values of nickel (II) state. Each Ni(II) ions are further interconnected by the adjacent Ni(II) ions by the alternate bridges, related with the inversion center, to form the infinite 1D Ni(II)-azide chain, with Ni···Ni distances of 5.09(1) Å and 3.23(1) Å, respectively (Figure 4). This alternate double EE and double EO azide-bridging chains has been found in a number of metal-azide compounds, but is very still rare for Ni(II) ones[12]. In the double EO bridged $Ni(N_3)_2Ni$ moiety, with a Ni-N-Ni angle of 98.75(6)°, the Ni-N-Ni-N ring is strictly planar due to the existence of the inversion center. The double EE moiety adopts a chair conformation, with a dihedral angle of 31.1° between the $(N_3)_2$ plane and the N–Ni–N plane.

For **2**, the inherently flexible tetrapyridyl ligand 4-TPOM ligand adopts a highly distorted bowl-like conformation of the four pyridyl groups on the same side of the central atom. Each 4-TPOM ligand utilizes two pyridyl arms to ligate two neighboring Ni(II) ions as the double EE bridged $Ni(N_3)_2Ni$ moiety in one nickel-azide chain, and the remaining two arms bind another double EE bridged $Ni(N_3)_2Ni$ moiety of different nickel-azide chain, shown in Figure 5. The $N\cdots C_{central}\cdots N$ angles ranging from 74.33(10)º to 131.98(10)º. To adapt to the distorted configuration of the tetra-pyridyl ligand, the different nickel-azide chains are distributed in the nearly perpendicular directions with the angle of 85.9°. The chains in different orientations are arrayed alternately to form a 2D crystal plane connected by 4-TPOM ligand, and further extended by other ligands to form a 3D network.

To survey the whole structure conveniently, the central quaternary carbon atom (C13) and the double EO bridged $Ni(N_3)_2Ni$ moiety are separately assumed as 4,4-connected nodes: Considering each central carbon atom C13 is connected to four double EE bridged $Ni(N_3)_2Ni$ moiety, and double EO bridged $Ni(N_3)_2Ni$ moieties is further connected to two C13 nodes and two $Ni(N_3)_2Ni$ moieties (through double EE bridges), the structure of **2** should possess a uninodal 4-connected *cds* net with the point (Schläfli) symbol $\{6^5\cdot8\}$.[13] This net was simplified to analyze supernet-subnet relations by *TOPOS* as subnet of the 4-connected topology, and has been observed in CPs.

Crystal structure of 3

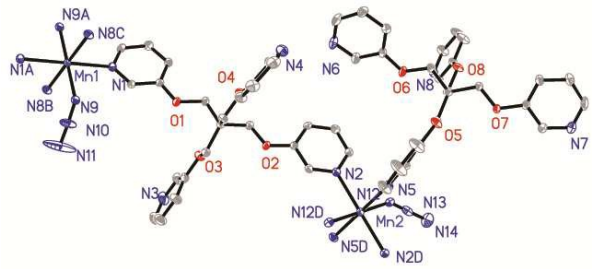

Figure 5. the perspective view of asymmetric unit of **3** with 30% probability level (hydrogen atoms were omitted for clarity).

The X-ray single crystal diffraction study indicates that **3** crystallizes in the monoclinic crystal system $P2_1/c$, and shows a two dimensional layer structure resulting from the connecting of manganese atoms through slightly-distorted cross-shaped 3-TPOM ligand. The asymmetric unit contains two Mn ions located on a crystallographic inversion centers, two independent azide ions, two independent 3-TPOM ligands and lattice molecules as water and methanol molecules(Figure 5). The central manganese atom adopts the octahedral geometry and is coordinated by six N atoms. The equatorial positions are

occupied by four pyridyl rings of different tetra-pyridinate ligands, while the axial positions are occupied by two coordinated azide ions, shown in Figure 7.The Mn-$N_{pyridine}$ and -N_{azide} bond lengths fall in regions of 2.156 to 2.340 Å, respectively, in accordance with the typical values of Mn(II) state.

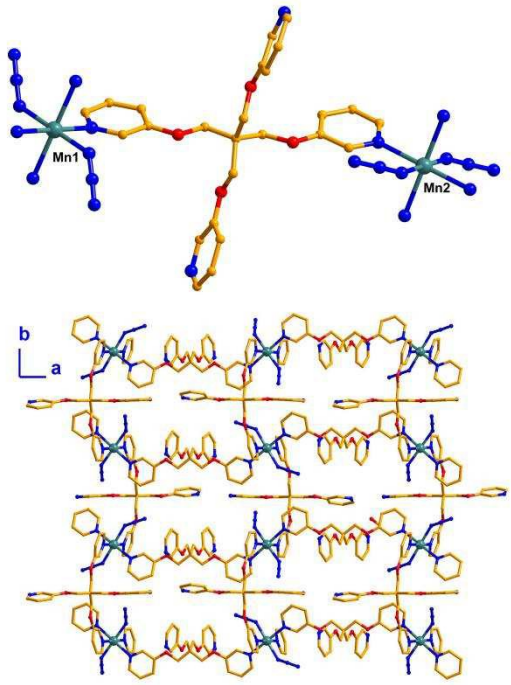

Figure 6. Up) the coordination modes of the tetra-pyridinate ligand and the central Mn ions; down) 2D structure of compound **3** (hydrogen atoms are omitted for clarity).

For **3**, the two types of inherently flexible tetrapyridyl ligand 3-TPOM ligands adopt slightly distorted center-symmetric cross-shaped configuration. Each 3-TPOM ligand interconnects two Mn atoms via its opposite pyridyl rings located on the same side compared to the central carbon atom (Figure 6) to form the 2D sandwiched layer. The first type of 3-TPOM ligands with N···$C_{central}$···N angles ranged from 172.14(3)º to 177.84(2)º utilize to connect two different Mn atoms to form the 1D chains along *a*-axis direction. The 1D Mn-3-TPOM chains are capped by the second-type 3-TPOM ligands with N···$C_{central}$···N angles ranged from 134.14(3)º to 176.57(2)º to form the 2D sandwich layer in *ab* plane, shown in Figure 6. Each layer is further connected by the adjacent layers via the C-H···π interactions with the distance of 2.824Å to form the 3D supramolecular structure.

To survey the whole structure conveniently, the central quaternary carbon atom and the Mn atoms are separately assumed as 2- and 4-connected nodes: Considering each central carbon atom is connected to two Mn atoms, and each Mn ion is further connected to four carbon nodes, the 2D sheet structure of **3** should possess a novel uninodal 4-connected *sql/Shubnikov* tetragonal net with stoichiometry (4-c) and the point (Schläfli) symbol $\{4^4\cdot6^2\}$.[13] Thus interleaved *sql/Shubnikov* tetragonal planes net stack over each other along the *c* axis direction. Interestingly, a [4] tiling structure with plane net signature of $[121]_4[4\cdot4\cdot4\cdot4]$ is further presented, which not only tends to decrease the pore volume, but stabilize the whole crystal structure through weak interactions.

Crystal structure of 4

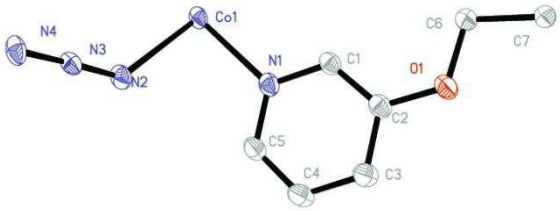

Figure 7. the perspective view of asymmetric unit of **4** with 30% probability level (hydrogen atoms were omitted for clarity).

The X-ray single crystal diffraction study indicates that **4** crystallizes in the tetragonal crystal system $I4_1/a$, and shows a three dimensional structure resulting from the connecting of 1D Co^{II}-azide neutral chains with double EE azide bridges through cross-shaped 3-TPOM ligand. The asymmetric unit contains a cobalt ion located on a crystallographic inversion center, one independent azide ion and quarter 3-TPOM ligand (Figure 7). The central cobalt atom adopts the octahedral geometry. The axial positions are occupied by two pyridyl rings of different tetra-pyridinate ligands, while the equatorial positions are occupied by four EE azide ions. The Co-$N_{pyridine}$ and Co-N_{azide} bond lengths fall in regions of 2.122 to 2.243 Å, respectively, in accordance with the typical values of cobalt(II) state. Each Co(II) ions are further interconnected by the adjacent Co(II) ions via the double EE azide bridges to form the infinite 1D Co(II)-azide chain, with Co···Co distances of 5.145(2) Å (Figure 8).

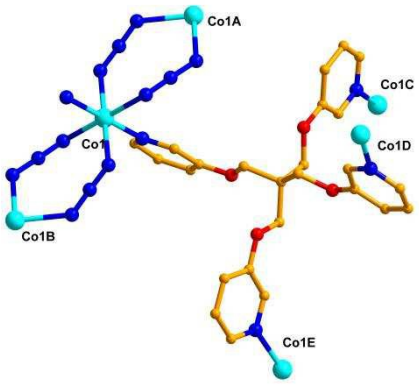

Figure 8. the coordination modes of the tetra-pyridinate ligand and the central Co ions in **4**.

For **4**, the inherently flexible tetrapyridyl ligand 3-TPOM ligand adopts a slightly distorted center-symmetric cross-shaped configuration with the range of N···$C_{central}$···N angle of 141.55(3)º. The opposite two pyridyl rings locate on the same side compared to the central carbon atom, and each pyridyl N atom coordinate to one cobalt ion of different 1D cobalt-azide chain (Figure 9) respectively to form the bilayer structure. In each layer, the 1D chain is parallel to each other, but perpendicular to other 1D cobalt-azide chains in the adjacent layers. The alternately directed 1D cobalt-azide chains are further extended by the connection of 3-TPOM ligands to form the 3D structure, leaving 1D channels along the *a*- and *b*-axial directions (Figure 9b), occupied by solvent molecules as methanol and water molecules. Calculated using the PLATON

routine, the solvent accessible volume in the dehydrated structure of **4** is about 22%.[14]

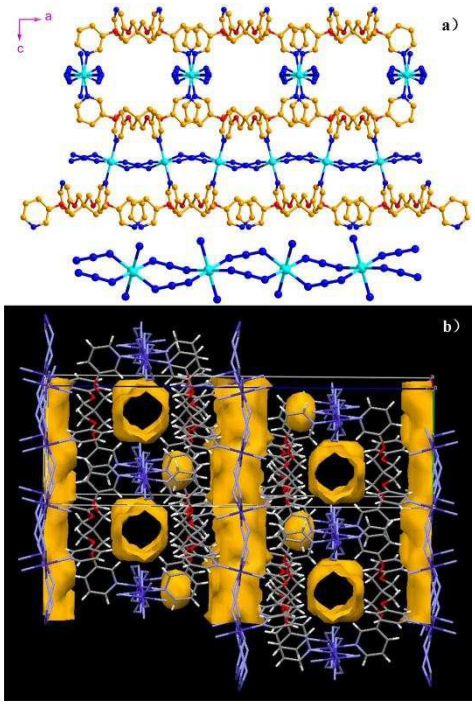

Figure 9. a) 3D structure of compound **4** (hydrogen atoms are omitted for clarity) along with the connection mode of 1D Co-N3 chain; b) the perspective view of the 1D channels of 4.

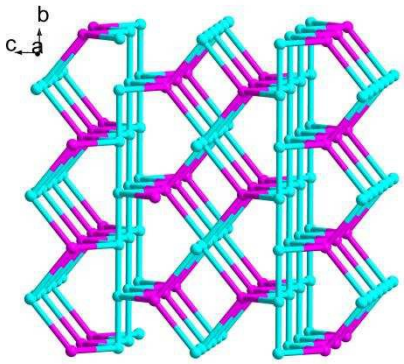

Figure 10. The ball-stick diagram of the topology of 4: green and purple balls represent the Co2 and 3-TPOM centers.

To survey the whole structure conveniently, the central quaternary carbon atom (C7) and the double EE bridged $Co(N_3)_2Co$ moiety are separately assumed as 4-connected nodes: Considering each central carbon atom C13 is connected to four Co atoms, and each Co ion is further connected to two C7 nodes and two Co (through double EE bridges), the structure of **4** should possess a novel binodal 4, 4-connected net with stoichiometry $(4\text{-c})(4\text{-c})_2$ and the point (Schläfli) symbol $\{6^2\cdot7^4\}\{6^4\cdot7\cdot9\}_2$.[13] This net was simplified to analyze supernet-subnet relations by *TOPOS* as subnet of the 4,4-connected topology, and has never been observed in CPs (Figure 10).

Magnetic properties of 2 and 4

The variable-temperature magnetic susceptibilities of **1-4** were measured on crystalline samples under 1 kOe in the range of 2–300 K and are shown as $\chi_M T$ and χ_M versus T plots in Figures 11, 14 and S5, respectively. Due to the lack of effective bridging azide ions, mainly paramagnetic behaviors of **1** and **3** were presented as shown in Figure S5.

The $\chi_M T$ value of **2** at 300 K is about 1.91 emu K mol^{-1}, similar to the experimental value of the spin-only value (2 emu K mol^{-1} from g = 2.00) expected for two magnetically isolated Ni^{II} ions. As the temperature is lowered, the $\chi_M T$ value decreases continuously down to 1.62 emu K mol^{-1} at 100 K. Then the $\chi_M T$ value increases rapidly up to a maximum value of 4.51 emu K mol^{-1} at 35 K. Upon a further decrease of the temperature lower than 35 K, the $\chi_M T$ value drops rapidly to 0.35 emu K mol^{-1} at 2K, suggesting antiferromagnetic interactions between the chains or the saturation effect. The upturn of $\chi_M T$ value below 100 K suggests an uncompensated magnetic moment of the system possibly arising from spin canting of the antiferromagentically coupled Ni(II) ions.[15] The data above 100 K follow the Curie–Weiss law with C = 2.7 emu K mol^{-1} and θ = –91.8 K. The above characteristics clearly suggest overall antiferromagnetic interactions between Ni^{II} ions in compound **2**.

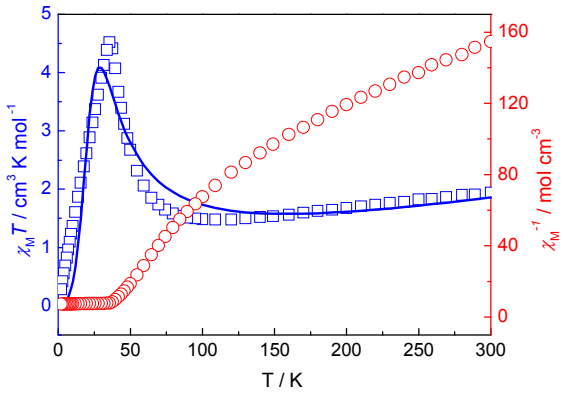

Figure 11. $\chi_M T$ and χ_M versus T plots of **2** in the temperature range of 2-300 K under 1 kOe.

It is noticeable that the magnetic susceptibility shows strong field dependence below 43 K. By applying different magnetic fields, the magnetic susceptibility increases with decreasing magnetic field because of small spontaneous magnetization of canted antiferromagnetism.[15] In order to characterize the low-temperature behaviors, the field-cooled (FC) and zero-field-cooled (ZFC) magnetizations were measured at 200 Oe upon warming from 2 K to 50 K(Figure 12) . The ZFC and FC plots completely diverge below 38 K, suggesting the onset of long-range ordering. The temperature dependencies of ac magnetic susceptibility under H_{dc}=0 Oe and H_{ac}= 3Oe had also been measured with frequencies of 1 and 1488 Hz from 2 to 50 K, no significant in-phase and out-phase ac signal signals could be detected (Figure S1).

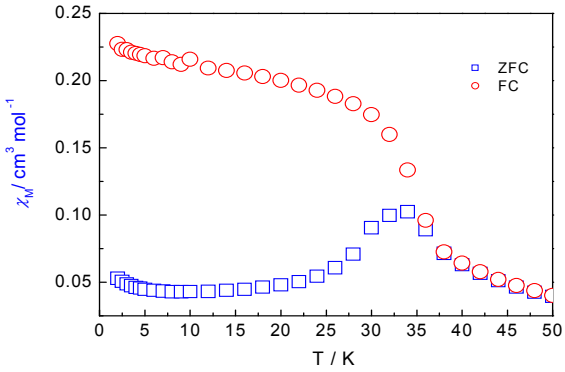

Figure 12. ZFC and FC magnetization of **2** at 200 Oe warming from 2 K to 50 K

The field-dependent magnetization of **2** shows a distinct sigmoid shape, manifesting the occurrence of a magnetic transition induced by the external field (Figure 13). The transition field is calculated as 2.0 kOe determined by a d*M*/d*H* derivative curve. The magnetization at 70 kOe is 1.54 *Nβ*, much lower than the expected saturation value of 4.0 *Nβ* anticipated for two Ni(II) ions with *S*=1 spins with *g*=2.0, indicating the overall antiferromagnetic couplings between Ni(II) ions. A hysteresis loop is observed clearly at 2.0 K giving a coercive field of $H_c \approx$ 1.8 kOe and a remnant magnetization of M_r= 0.66 *Nβ*. (Figure S2 in the Supporting Information). The canting angle can then be estimated to be about 9.37° based on the equation[15] $\alpha = \tan^{-1}(M_r/M_s)$.The large angle of spin canting could be also found in other azide-systems.[15]

Referring to the above magnetic measurements, **2** might display spin-canted antiferromagnetic behavior, which may originate from the single-ion anisotropy of Ni(II).[15] The possible structural phase transition was excluded due to no peak could be observed in the low temperature heat capacity(Figure s7). Because the presence of an inversion center between Ni ions in **2** with space group *C2/c* forbids the occurrence of antisymmetric exchange interaction.

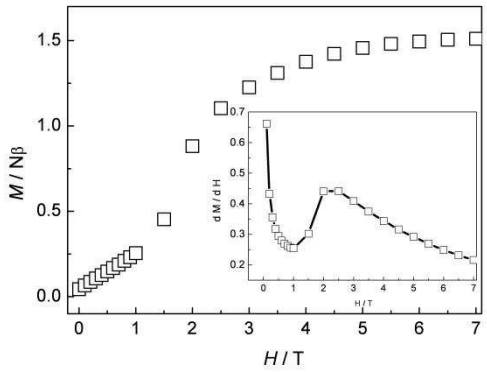

Figure 13. field dependence of the magnetization for **2** (Inset: dM/dH vs. H plot.)

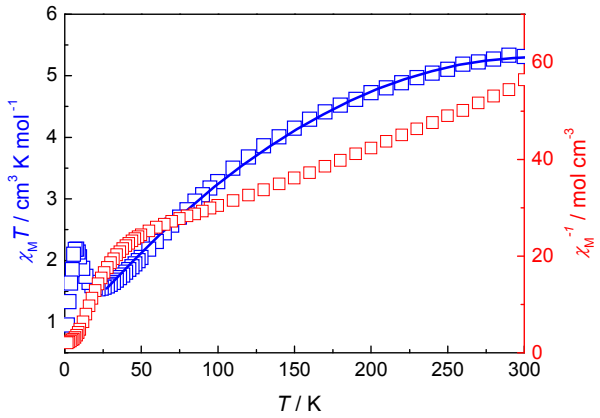

Figure 14.χ_MT and χ_M versus T plots of **4** in the temperature range of 2-300 K under 1 kOe

With the consideration of the structural characteristic of **2**, the model could be seen as chains with alternating *J*1 and *J*2 interactions through the alternating double EO and double EE azide bridges. To roughly stimulate the magnetic interactions, the classical theoretical spin model for the chains with alternating *J*1 and *J*2 interactions was adopted.[16] Based on the spin Hamiltonian given in equation 1, the expression of magnetic susceptibility per spin site for such systems has been deduced as equation 2 with u_i= coth[J_iS(S+1)/*k*T]-*k*T/[*Ji*S(S+1)] and *S* = 1. The best fit of the experimental data gave J_1 = 77 cm^{-1}, J_2 = -83 cm^{-1} and g = 2.39. The positive J_1 value indicates ferromagnetic coupling interaction between EO-azide-bridged Ni(II) ions, while negative J_2 suggests antiferromagnetic interaction between EE-azide-bridged Ni(II) ions, in accordance with other reported systems.

$$H = -J_1 \sum S_{2i} S_{2i+1} - J_2 \sum S_{2i+1} S_{2i+2} \quad (1)$$

$$\chi = [\mathrm{N}g^2\beta^2 S(S+1)/(3kT)][(1+u_1+u_2+u_1u_2)/(1-u_1u_2)] \quad (2)$$

$$\chi = \mathrm{N}g^2\beta^2 S(S+1)(1+u)/3kT(1-u) \quad (3)$$

The $\chi_M T$ value of **4** at 300 K is about 5.35 emu K mol^{-1}, higher than the experimental value of the spin-only value (3.75 emu K mol^{-1}) expected for two magnetically isolated high-spin d^7 Co^{II} ions, which might be caused by the unquenched orbital contributions for octahedral Co(II) ions or magnetic interactions between Co(II) ions.[15] As the temperature is lowered, the $\chi_M T$ value decreases continuously down to 1.54 emu K mol^{-1} at 22 K. Then the $\chi_M T$ value increases rapidly up to a maximum value of 2.19 emu K mol^{-1} at 8 K. Upon a further decrease of the temperature lower than 8 K, the $\chi_M T$ value drops rapidly to 0.95 emu K mol^{-1} at 2K because of the saturation effect. The magnetic susceptibilities of **4** do not show field-dependent behavior. The data above 100 K follow the Curie–Weiss law with *C* = 1.66 emu K mol^{-1} and θ = –90.6 K. The above characteristics clearly suggest overall antiferromagnetic interactions between Co^{II} ions in compound **4**. No long range ordering and hysteresis phenomenon could be detected to validate the existence of spin canting behavior of **4**.

With the consideration of the structural characteristic of **4**, the model could be seen as chains with *J* interactions through the double EE azide bridges. Usually, the magnetic fitting of Co(II) systems is difficult due to the large anisotropy caused by spin-orbital coupling. For 4, the simplest spin model as equation 3 was adopted with S = 3/2 and *u* = -coth[*k*T/12*J*] + *k*T/12*J*.[17] The best fit of the experimental data above 30 K gave *J* = - 34 cm^{-1} and g = 2.26. The negative *J* suggests

antiferromagnetic interaction between EE-azide-bridged Co(II) ions, in accordance with other reported systems.

Conclusions

In conclusion, by introduction of the flexible tetra-pyridinate ligands, 4-TPOM and 3-TPOM, four azide-containing Mn(II), Co(II) and Ni(II) coordination polymers have been synthesized and characterized structurally and magnetically. Due to the different flexibilities of the tetra-pyridinate ligands, a series of diverse structures was obtained. **1** shows 1D helical chain comprised of six-coordinated Mn^{II} geometries and two-connected tetra-pyridinate ligands. Compound **2** exhibits a three-dimensional framework based on 1D Ni(II) chains with alternating double end-to-end (EE) and double end-on (EO) azide bridges and tetrapyridyl ligands in a highly-distorted conformation. Compound **3** shows 2D layer comprised of six-coordinated Mn^{II} geometries with mono-dentate azide ions and two types of two-connected tetra-pyridinate ligands. Compound **4** exhibits a three-dimensional framework based on 1D Co(II) chains with double end-to-end (EE) azide bridges and tetrapyridyl ligands in a cross-shaped conformation. In addition, complex **2** might exhibit spin-canted weak antiferromagnetic properties. The occurrence of spin canting may originate from the single-ion anisotropy of Ni(II) or possible structural phase transition. In complex **4**, overall antiferromagnetic exchange interactions are observed, and no long-range ordering exists above 2.0 K. This article demonstrates that azide could be a powerful building unit to construct three dimensional molecule-based magnets, and the combination of flexible tetra-pyridinate coligands and azido could result in variable three dimensional structures, which would provide more novel azide-containing compounds to investigate fascinating magnetic behaviors.

Acknowledgements

Professor Jun Tao in Xiamen University must be thanked for his great guidance. We gratefully acknowledge the National Natural Science Foundation of China (no.21471062, 21101066) , Wuhan Science and Technology Bureau (no. 201271031382, 201271031384) and) and Students' scientific research project of Jianghan university(No. 277-6) for financial support, and the Analytical and Testing Center, Huazhong University of Science and Technology for analysis and spectral measurements.

Notes and references

[a] Key Laboratory of Optoelectronic Chemical Materials and Devices of Ministry of Education,School of Chemical and Environmental Engineering, Jianghan University, Wuhan 430056, PR China. Email:yufan0714@163.com

[b] School of Chemistry and Chemical Engineering, Huazhong University of Science and Technology, Wuhan, Hubei 430074, PR China. Email:libao@hust.edu.cn

Electronic Supplementary Information (ESI) available: the detailed synthesis procedure, magnetic properties and crystal cif files . See DOI: 10.1039/b000000x/

1 (a) M. Kurmoo, *Chem. Soc. Rev.*, 2009, **38**, 1353; (b) X.-Y. Wang, Z.-M. Wang and S. Gao, *Chem. Commun.*, 2008, 281; (c) Y.-F. Zeng, X. Hu, F.-C. Liu and X.-H. Bu, *Chem. Soc. Rev.*, 2009, **38**, 469; (d) J. Ribas, A. Escuer,M.Monfort, R. Vicente, R. Cortés, L. Lezama and T. f. Rojo, *Coord. Chem. Rev.*, 1999, **193–195**, 1027;(e)J. W. Shin, J. M. Bae, C. Kim, K. S. Min, *Dalton Trans.*, 2014, **43**, 3999; (f)T. Biet, N. Avarvari, *CryEngComm*, 2014, **16**,6612.

2 (*a*) J. Ribas, A. Escuer, M. Monfort, R. Vicente, R. Cortes, L. Lezama and T. Rojo, *Coord. Chem. Rev.*, 1999, **193–5**, 1027 ; (*b*) C. Adhikary and S. Koner, *Coord. Chem. Rev.*, 2010, **254**, 2933 ; (*c*) K. S. Lim, D. W. Ryu, W. R. Lee, E. K. Koh, H. C. Kim and C. S. Hong, *Chem.–Eur. J.*, 2012, **18**, 11541;(d) Z. Meng, L. Yun, W. Zhang, C. Hong,R. Herchel, Y. Ou,J. Leng, M. Peng, Z. Lin, M. Tong, *Dalton Trans.*, 2009, 10284;(e) S. Mukherjee, P. S. Mukherjee, *Account Of Chmeical Research*, 2013, **46**, 2556; (f) A. J. Calahorro, A. Salinas-Castillo, J. M. Seco, J. Zuniga, E. Colacio, A. Rodriguez-Dieguez, *CryEngComm*, 2014, **15**, 7636.

3 (*a*) X. Y. Wang, Z. M. Wang and S. Gao, *Sci. China Chem.*, 2012, **55**, 1055 ; (*b*) E. Q. Gao, A. L. Cheng, Y. X. Xu, M. Y. He and C. H. Yan, *Inorg. Chem.*, 2005, **44**, 8822; (*c*) E. Q. Gao, P. P. Liu, Y. Q. Wang, Q. Yue and Q. L. Wang, *Chem.–Eur. J.*, 2009, **15**, 1217; (*d*) R. Biswas, S. Mukherjee, P. Kar and A. Ghosh, *Inorg. Chem.*, 2012, **51**, 8150; (e) S. Goswami, S. Sanda, S. Konar, *CryEngComm*, 2014, **15**, 369.

4 (*a*) S. Q. Bai, C. J. Fang, Z. He, E. Q. Gao, C. H. Yan and T. S. A. Hor, *Dalton Trans.*, 2012, **41**, 13379; (*b*) S. Biswas, S. Naiya, C. J. Gomez-Garcia and A. Ghosh, *Dalton Trans.*, 2012, **41**, 462 ; (*c*) S. Mukherjee, Y. P. Patil and P. S. Mukherjee, *Dalton Trans.*, 2012, **41**, 54 ; (*d*)C.-I. Yang, Y.-J. Tsai, S.-P. Hung, H.-L. Tsai and M. Nakano, *Chem. Commun.*, 2010, **46**, 5716.

5 (a) X. H. Liu, M. Krott, P. Müller, C. H. Hu, H. Lueken and R. Dronskowski, *Inorg. Chem.*, 2005, **44**, 3001; (b) W. P. Liao, C. H. Hu, R. K. Kremer and R. Dronskowski, *Inorg. Chem.*, 2004, **43**, 5884; (c) W. P. Liao and R. Dronskowski, *Inorg. Chem.*, 2006, **45**, 3828; (d) R. Srinivasan,M. Ströbele and H. J. Meyer, *Inorg. Chem.*, 2003, **42**, 3406.

6 (a) P. Gütlich, Y. Carcia and H. A. Goodwin, *Chem. Soc. Rev.*, 2000, **29**, 419; (b) P. Gütlich and H. A. Goodwin (Editors), *Top. Curr. Chem.*, 2004, **233** ; (c) A. B. Gaspar, V. Ksenofontov, M. Seredyuk and P. Gütlich, *Coord. Chem. Rev.*, 2005, **249**, 2661.

7 (a) Z. L. Lu, M. Yuan, F. Pan, S. Gao, D. Q. Zhang and D. B. Zhu, *Inorg. Chem.*, 2006, **45**, 3538; (b) X. Y. Wang, B. L. Li, X. Zhu and S. Gao, *Eur. J. Inorg. Chem.*, 2005, 3277.

8 (a) P. J. Hagrman, D. Hagrman and J. Zubieta, *Angew. Chem., Int. Ed.*, 1999, **38**, 2638; (b) S. J. Han, J. L. Manson, J. Kim and J. S. Miller, *Inorg. Chem.*, 2000, **39**, 4182; (c) A. K. Ghosh, D. Ghoshal, E. Zangrando, J. Ribas and N. R. Chaudhuri, *Inorg. Chem.*, 2005, **44**, 1786.

9 Y. Wang, Q. Sun and En-Qing Gao, *Inorg. Chem. Comm.*, 2012, **15**, 8.

10 (a) L. L. Liang, Sh. B. Ren, J. Zhang, Y. Zh. Li, H. B. Du, X. Z. You, *Cryst. Growth Des.*, 2010, **10** , 1307; (b) J. S. Hu, Y. J. Shang, X. Q. Yao, L. Qin, Y. Zh. Li, Z. J. Guo, H. G. Zheng, Z. L. Xue, *Cryst. Growth Des.*, 2010, **10** , 2676 ; (c)S.-B. Ren, L. Zhou, J. Zhang, Y.-Zh. Li, H.-B. Du, and X.-Z. You, *CrystEngComm*, 2009, **11**, 1834; (d) S.-B. Ren, L. Zhou, J. Zhang, Y.-L. Zhu, Y.-Zh. Li, H.-B. Du and X.-Z. You, *CrystEngComm.*, 2010, **12**, 1635; (e) Q. Zhang, X. Bu, Z. Lin, T. Wu, P. Feng, *Inorg. Chem.,* 2008, **47**, 9724; (f) J. Guo, J.-F. Ma, B. Liu, W.-Q. Kan and J. Yang, *Cryst. Growth Des.*, 2011, **11** , 3609.

11 (a) B. Li, L. Q. Chen, R. J. Wei, J. Tao, R. B. Huang, L. S. Zheng, Z. Zheng, *Inorg. Chem.* 2011, **50**, 424; (b) F. Yu and B. Li, *CrystEngComm*, 2011, **13**, 7025; (c) F. Yu, W. Yu, B. Li and T. Zhang, *CrystEngComm*, 2012, **14**, 6770; (d) F. Yu and B. Li, *CrystEngComm*, 2012, **14**, 6049; (f) W. Yu, F. Yu, B. Li and T. Zhang, *CrystEngComm*, 2012, **14**, 8396.

12 (a) M. Monfort, I. Resino and J. Ribas, *Inorg. Chem.* 2000, **39**, 2572; (a) X.-T. Wang, X.-H. Wang, Z.-M. Wang and S. Gao, *Inorg. Chem.* 2008, **48**, 1301.

13 V. A. Blatov, *IUCr CompComm Newsletter*, 2006, **7**, 4; see also http://www.topos.ssu.samara.ru.

14 A. L. Spek, PLATON, Utrecht University, Utrecht, The Netherlands, 1998.

15 (a) D.-F. Weng Z.-M. Wang, S. Gao, *Chem. Soc. Rev.* 2011, **40**, 3157; (b) J. Li, B. Li, P. Huang, H.-Y. Shi, R.-B. Huang, L.-S. Zheng and J. Tao, *Inorg. Chem.* 2013, **52**, 11573; (c) C. Bellitto, F. Federici, M. Colapietro, G. Portalone, D. Caschera, *Inorg. Chem.* 2002, **41**, 709.

16 M. A. M. Abu-Youssef, M. Drillon,A. Escuer, M. A. S. Goher, F. A. Mautner, R. Vicente, *Inorg. Chem.* 2000, **39**, 5022.

17 M. E. Fisher, *Am. J. Phys.* 1964, **32**, 343.